

Evolving Afferent Architectures: Biologically-inspired Models for Damage-Avoidance Learning

Wolfgang Maass^{1,2}, Sabine Janzen², Prajvi Saxena², Sach Mukherjee^{3,4}

¹Saarland University, Saarbrücken, Germany

²German Research Center for Artificial Intelligence (DFKI), Saarbrücken, Germany

³Statistics and Machine Learning, German Center for Neurodegenerative Diseases (DZNE), Bonn, Germany

⁴MRC Biostatistics Unit, University of Cambridge, Cambridge, UK

February 5, 2026

Abstract

We introduce *Afferent Learning*, a framework that produces *Computational Afferent Traces* (CATs) as adaptive, internal risk signals for damage-avoidance learning. Inspired by biological systems, the framework uses a two-level architecture: evolutionary optimization (outer loop) discovers afferent sensing architectures that enable effective policy learning, while reinforcement learning (inner loop) trains damage-avoidance policies using these signals. This formalizes *afferent sensing* as providing an inductive bias for efficient learning: architectures are selected based on their ability to enable effective learning (rather than directly minimizing damage). We provide theoretical convergence guarantees under smoothness and bounded-noise assumptions. We illustrate the general approach in the challenging context of biomechanical digital twins operating over long time horizons (multiple decades of the life-course). Here, we find that CAT-based evolved architectures achieve significantly higher efficiency and better age-robustness than hand-designed baselines, enabling policies that exhibit age-dependent behavioral adaptation (23% reduction in high-risk actions). Ablation studies validate CAT signals, evolution, and predictive discrepancy as essential. We release code and data for reproducibility.

1 Introduction

Biological afferents are sensory pathways that convey information from the periphery to the central nervous system, based on a dual-level organization. At the *phylogenetic* level, afferent architectures are evolved to enable effective damage-avoidance learning; at the *ontogenetic* level, neural circuitry adapts over an organism’s lifetime to respond to afferent signals [2, 16]. This bi-level selection and optimization can be viewed as implementing a form of inductive bias with respect to learnability. Sensing archi-

tures are optimized to support efficient policy learning under risk rather than directly minimizing physical damage. This general schema of adaptive sensors coupled with bi-level phylogenetic and ontogenetic optimization is observed not only in the nervous system but across biology, including sensing and fine-tuning mechanisms in immunity and DNA damage sensing and repair.

In contrast, AI systems interacting with models of biological or biomedical systems typically lack internal signals that identify harmful states, integrate temporal stress accumulation, and store this information to bias future decisions. A key application, which motivates this work, is in biomedical digital twins (DTs). DTs in medicine have reached high fidelity [11], and their integration with AI approaches has high potential, but most applications remain reactive and memoryless, preventing adaptive damage-avoidance behaviors and this is an important factor that continues to limit their practical utility.

In this paper, motivated by the foregoing observations about biological systems, we introduce a class of AI architectures in which adaptive sensing mechanisms, termed *Computational Afferent Traces* (CATs), serve as internal risk signals intended to be operationally equivalent to afferent mechanisms in biological systems. We focus in particular on settings in which an embodied agent operates on tasks involving damage accumulation over time. As we see below, the CATs we learn are related to physiologically-plausible damage signals rather than only abstract considerations. The goal of the (computational) afferent mechanisms we propose is to endow AI systems with an internal risk indicator that guides adaptive behavior. For example, in the specific setting of a biomechanical DT, we would expect CATs to capture aspects such as non-physiological load, instability-driven stress or cumulative strain and thereby allow efficient learning,

Specifically, we propose a learning architecture that mirrors the bi-level (phylogenetic/ontogenetic) organization

of biological afferents: evolutionary optimization (outer loop) discovers afferent sensing architectures that enable effective policy learning [10, 19], while reinforcement learning (inner loop) trains damage-avoidance policies using these signals [22]. This separation enables afferents to provide an inductive bias with respect to learnability, where architectures are selected based on their ability to enable effective learning (rather than directly minimizing damage).

2 Related Work

Artificial afferents have been investigated primarily in the context of neurorobotics and bio-inspired sensing, where afferent signals are used to trigger reflexive behaviors or protective responses [7, 24]. In parallel, musculoskeletal digital twins integrate medical imaging, biomechanical modeling, and finite-element simulation to analyze tissue stress, degeneration, and injury risk [6, 11]. While these approaches provide important diagnostic and predictive capabilities, they typically treat afferent inputs or damage as an external quantity to be estimated rather than as an internal, learned risk state that actively shapes behavior and learning over time.

A complementary line of work models afferent inputs as an inferential process that integrates sensory evidence, prior expectations, and uncertainty providing an internal belief or risk-related latent state that influences perception and action selection [3, 9, 23]. Although conceptually aligned with the notion of afferent internal signals, these models are often underspecified at the algorithmic level and are rarely grounded in explicit biomechanical damage processes or evaluated in long-horizon learning and control scenarios.

Episodic memory has been shown to improve decision-making, planning, and adaptation in artificial agents [5, 15, 18]. However, episodic mechanisms in reinforcement learning are typically grounded in abstract state-action-reward representations rather than physics-based damage or wear signals [17]. As a result, episodic recall is seldom used to anticipate biomechanical risk or long-term structural degradation.

Hierarchical and meta-learning frameworks separate architectural optimization from policy learning [20, 21]. In reinforcement learning, evolutionary strategies have been employed as outer-loop optimizers [10, 19], while gradient-based methods such as PPO are commonly used for policy learning [22]. In contrast to approaches that directly evolve policies or rewards, our method evolves afferent sensing architectures whose fitness is evaluated based on downstream learning outcomes. While our approach shares some motivation with general meta-learning, in contrast to established meta-learning frameworks such

as MAML and variants [8, 12, 14] our focus is not on general heuristics concerning learning dynamics but rather specific adaptive sensors and their integration via bi-level phylogenetic/ontogenetic-like learning. Furthermore, we focus specifically on the setting of agents operating in tasks involving damage accumulation over time, where the particular inductive bias we propose is a natural computational analogue to real, biological damage-sensing mechanisms and associated adaptation.

3 Core Architecture for Computational Afferent and Adaptive Learning

This section outlines the core concepts of the architecture; implementation details are deferred. For concreteness, we use biomechanical digital twins (BDTs) as a running example. We consider an embodied agent in a simulated environment with cumulative damage. At each time step t , the environment provides observations $x_t \in \mathbb{R}^K$ under action a_t and context s_t . The agent maintains an internal, unobservable damage state $D_t \in \mathbb{R}_{\geq 0}$ that accumulates with mechanical loading, inducing partial observability that is addressed through afferent sensing.

3.1 Computational Afferent Traces (CATs)

Definition 1 (Computational Afferent Trace (CAT)). Let $x_t \in \mathbb{R}^K$ denote the feature vector at time t , a_t the agent action, and s_t optional contextual parameters. A *Computational Afferent Trace (CAT)* is an internal scalar signal

$$c_t \in [0, 1]$$

that encodes the predicted mechanical risk associated with the current state-action pair.

The concrete architecture we propose comprises an *afferent array* parameterized by ϕ , consisting of M units. Each *afferent unit* i computes a projected signal

$$u_i(t) = w_i^\top x_t,$$

where $w_i \in \mathbb{R}^K$ is a unit-normalized feature projection. The afferent activation $a_i(t)$ evolves according to a stable first-order autoregressive (AR(1)) process with a thresholded nonlinear innovation term:

$$a_i(t) = (1 - \beta_i) a_i(t - 1) + \beta_i \sigma(\alpha_i(u_i(t) - \theta_i)),$$

where $\alpha_i > 0$ is a gain parameter, θ_i is a learned activation threshold, $\sigma(\cdot)$ is a sigmoid nonlinearity, and

$$\beta_i = \frac{\Delta t}{\tau_i + \Delta t}, \quad \tau_i > 0,$$

defines the afferent time constant. This leaky-integrator dynamic ensures that afferent activations persist under sustained supra-threshold signals and decay otherwise. Finally, the CAT is computed as

$$c_t = \sum_{i=1}^M v_i a_i(t),$$

where aggregation weights satisfy $v_i \geq 0$ and $\sum_{i=1}^M v_i = 1$. The CAT implements thresholded autoregressive integration, enabling afferents to respond selectively to sustained excursions beyond evolved safety envelopes. This temporal integration provides persistence under sustained damage while allowing decay when damage-causing events subside.

3.2 Bi-Level Learning Architecture

The framework adopts a bi-level learning architecture inspired by the dual (phylogenetic/ontogenetic) organization of biological afferents. An *outer loop* evolves afferent sensing architectures to support effective policy learning, while an *inner loop* trains damage-avoidance policies using these signals. This separation selects afferent architectures for *learnability*, providing an inductive bias for policy learning rather than directly optimizing damage.

The architecture comprises three components: (i) an *environment* producing state observations x_t and an unobservable damage state D_t , (ii) an *Afferent Foundation Model (AFM)* that maps (x_t, s_t) to Computational Afferent Traces (CATs) via evolved afferent arrays, and (iii) an *Artificial Mental Model (AMM)* that stores and retrieves damage-related experiences for behavioral modulation. Policies π_θ are learned over a lifetime, while afferent architectures are optimized across evolutionary time.

4 Afferent Foundation Model (AFM)

We formalize afferent sensing as an evolved inductive bias that shapes learning in embodied systems. We now turn attention to an Afferent Foundation Model (AFM) that processes state observations x_t to produce CAT signals for guidance of policy learning.

4.1 Environment and Damage Dynamics

At each time step t , the environment produces state observations $x_t \in \mathbb{R}^K$, comprising normalized features (e.g., in the BDT context, features such as mechanical stress, strain, strain rate, shear, contact pressure, damage proxies, temporal patterns). The agent selects an action $a_t \sim \pi_\theta(\cdot | o_t)$ according to its policy, where o_t denotes the observation

vector that augments the state x_t with afferent signals (individual afferent activations and the aggregated CAT signal), inducing a state transition $x_t \rightarrow x_{t+1}$.

The environment maintains an internal damage state $D_t \in \mathbb{R}_{\geq 0}$:

$$D_{t+1} = D_t + g(x_t, a_t, D_t),$$

where $g(\cdot)$ encodes domain-specific damage accumulation (in the BDT context, D accumulates as a function of mechanical loading and g captures aspects such as fatigue, micro-tears, constraint violations etc.). The damage state D_t is *not directly observable* by the policy, creating a partial observability problem that afferent learning addresses.

4.2 Afferent Array Architecture

An *afferent array* is a distributed sensing system of M afferents (individual afferent pathways) that collectively monitor damage signals. The array operates as an ensemble: each afferent independently processes input features and produces an activation signal, and these signals are aggregated into a unified risk assessment.

We parameterize the afferent sensing architecture by $\phi \in \Phi$, which defines how potentially harmful internal states are sensed and encoded. The architecture consists of M afferent units, each computing a temporally integrated activation signal.

All afferents in the array receive the same feature vector x_t extracted from the environment, but each afferent specializes through its own learned feature projection and is hence adaptive. Each afferent $i \in \{1, \dots, M\}$ processes x_t and computes an activation $a_i(t)$ through three steps: (i) feature projection via a learnable weight vector $w_i \in \mathbb{R}^K$ (normalized to unit length), which enables each afferent to detect different patterns in the shared feature space, (ii) thresholded nonlinearity with gain $\alpha_i > 0$ and threshold $\theta_i \in [0, 1]$, and (iii) temporal integration with time constant $\tau_i > 0$. Following Sec. 3.1, the activation is updated as:

$$a_i(t) = (1 - \beta_i)a_i(t-1) + \beta_i \sigma(\alpha_i(w_i^\top x_t - \theta_i)),$$

where $\beta_i = \Delta t / (\tau_i + \Delta t)$ and $\sigma(\cdot)$ is a sigmoid nonlinearity. The first term provides long-term persistence, while the second term provides immediate response.

The afferent array can be viewed as a recurrent neural network layer with per-neuron parameters and temporal dynamics: it maps input $x_t \in \mathbb{R}^K$ to output activations $[a_1(t), \dots, a_M(t)] \in \mathbb{R}^M$ through learned projections w_i , with each afferent maintaining its own memory state $a_i(t-1)$ through the leaky-integrator dynamics. This temporal integration enables the array to maintain memory over time, similar to LSTM cells, allowing afferents to respond to sustained threats while decaying when threats subside.

The array operates as a parallel ensemble of M specialized detectors, each with its own learned feature projection w_i , enabling the array to collectively monitor diverse threat patterns. Through evolution, different afferents learn to specialize on different feature patterns.

The afferent array is parameterized by

$$\phi = \{\{w_i, \alpha_i, \theta_i, \tau_i\}_{i=1}^M, \{v_i\}_{i=1}^M\},$$

where $v_i \geq 0$ are aggregation weights (normalized: $\sum_i v_i = 1$) used to compute the aggregate afferent signal. The entire array configuration ϕ is evolved together as a unit (see Section 4.5), rather than training individual afferents separately; all afferents receive the same biomechanical feature vector x_t but specialize through their distinct learned projections w_i .

4.3 Computational Afferent Trace (CAT)

Afferent activations from a single afferent array are aggregated into a scalar internal signal termed the *Computational Afferent Trace* (CAT):

$$\text{CAT}(t) = \sum_{i=1}^M v_i a_i(t) \in [0, 1],$$

where the summation is over all M afferents in the array at time step t . The CAT serves as an internal cost signal that reflects the predicted harmfulness of the current state-action pair. CAT influences learning through two pathways: (i) as a penalty term in the reward signal (Equation 4), and (ii) as part of the policy’s observation space, enabling the policy to observe CAT patterns and learn to avoid high-CAT states. This integration enables the agent to learn damage-avoidance behaviors through reinforcement learning.

4.4 Policy Learning with Afferent Signals

The policy $\pi_\theta(a_t | o_t)$ is trained using Proximal Policy Optimization (PPO), where the observation augments physical state information with afferent signals and, when episodic memory is enabled, episodic memory signals:

$$o_t = \begin{cases} o_t^{\text{epi}}, & \text{episodic memory enabled,} \\ o_t^{\text{base}}, & \text{otherwise,} \end{cases} \quad (1)$$

$$o_t^{\text{epi}} = [x_t, a_1(t), \dots, a_M(t), \text{CAT}(t), \hat{y}_t, d_t], \quad (2)$$

$$o_t^{\text{base}} = [x_t, a_1(t), \dots, a_M(t), \text{CAT}(t)]. \quad (3)$$

Here, $o_t^{\text{epi}} \in \mathbb{R}^{K+M+3}$ and $o_t^{\text{base}} \in \mathbb{R}^{K+M+1}$, where \hat{y}_t is the recall risk signal from episodic memory (see Section 4.7) and d_t is the mean distance to retrieved episodes.

The afferent system and episodic memory influence action selection through two pathways: (i) the policy observes CAT patterns and episodic memory signals (\hat{y}_t, d_t) in its observation space, enabling it to condition actions on these signals, and (ii) high CAT values and recall risk reduce reward through penalty terms (Equation 4), creating learning signals that shape the policy via policy gradient updates. Through PPO, the policy learns to associate high-CAT observations and high recall risk with negative reward, leading it to select actions that transition to lower-CAT states and avoid situations similar to past damage experiences. This learning occurs through gradient-based updates that maximize expected cumulative reward, effectively learning to avoid state-action pairs that yield penalties.

The policy is optimized to maximize the expected cumulative reward:

$$\mathbb{E} \left[\sum_{t=1}^T r_t \right],$$

with per-step reward

$$r_t = r_t^{\text{task}} - \lambda_{\text{CAT}} \cdot \text{CAT}(t) - \lambda_D \cdot \Delta D_t - \lambda_{\text{mem}} \cdot \hat{y}_t, \quad (4)$$

where:

- r_t^{task} is a *task-specific reward function* encoding task performance.
- $\lambda_{\text{CAT}} > 0$: penalty weight for predicted harm via CAT, enabling anticipatory behavior.
- $\lambda_D > 0$: penalty weight for realized damage increments $\Delta D_t = D_{t+1} - D_t$, ensuring optimization remains grounded in actual structural integrity.
- $\lambda_{\text{mem}} > 0$: penalty weight for recall risk \hat{y}_t from episodic memory (when enabled), enabling learning from past experiences by discouraging actions similar to those that led to damage in similar contexts.

As damage accumulates with time, more state-action pairs may trigger high CAT values, leading the policy to learn a more restricted action distribution that avoids these high-risk states. This time-dependent action restriction mirrors behavior observed in biological systems (e.g., in the biomechanical context, older individuals adopting more conservative movement patterns) and is also relevant for artificial systems (e.g., robots or machines in predictive maintenance scenarios, where wear and tear naturally constrains the operating envelope). The policy learns this restriction through experience rather than having it imposed a priori, enabling adaptive compensation for time-dependent (e.g. in the applied example, age-related) structural degradation.

After N training steps under a fixed afferent configuration ϕ , we obtain optimized policy parameters:

$$\theta^*(\phi) = \text{RLTrain}(\pi_\theta, \phi, N),$$

where $\text{RLTrain}(\pi_\theta, \phi, N)$ denotes training the policy π_θ using PPO for N steps with afferent configuration ϕ fixed, yielding optimized parameters θ^* .

4.5 Evolutionary Optimization of Afferent Parameters

We optimize the afferent parameters ϕ using an outer-loop evolutionary strategy (CMA-ES). The fitness of a configuration ϕ is evaluated *after* policy learning, measuring long-horizon performance over evaluation rollouts:

$$J(\theta^*(\phi), \phi) = \mathbb{E}_{\text{eval}}[P(\theta^*(\phi)) - \gamma_D \cdot D_{\text{total}}], \quad (5)$$

where $P(\theta^*(\phi))$ is task performance, D_{total} is cumulative damage, and $\gamma_D > 0$ is a weighting coefficient.

The evolutionary objective is:

$$\phi^* = \arg \max_{\phi \in \Phi} \mathbb{E}[J(\theta^*(\phi), \phi)],$$

where the expectation is over environment stochasticity, initial conditions, and RL training randomness. This formulation implements *selection on learning outcomes*: afferent architectures are favored if they enable the agent to learn behaviors that minimize long-term damage while maintaining task performance.

Thus, our framework implements a bi-level learning architecture: an *inner loop* where the policy π_θ learns damage-avoidance behaviors using afferent signals (lifetime/procedural learning, analogous to the ontogenetic level in biological systems), and an *outer loop* where the afferent architecture ϕ is evolved to maximize post-learning fitness (analogous to phylogenetic selection).

4.6 Theoretical Analysis

We connect our evolutionary optimization to established evolution strategies theory [10]. CMA-ES operates on a Gaussian-smoothed version of the noisy fitness landscape, where the smoothing inherent in the algorithm provides robustness to the stochastic noise from RL training (PPO with trajectory sampling, clipping, random seeds). The key insight is that *selection on learning outcomes* (optimizing ϕ based on post-learning performance $J(\theta^*(\phi), \phi)$) discovers architectures that enable more effective damage-avoidance learning, rather than architectures that directly minimize damage. Evolved configurations ϕ^* enable richer policy classes \mathcal{H}_{ϕ^*} that contain hand-designed classes $\mathcal{H}_{\phi_{\text{hand}}}$, allowing policies to learn damage-avoidance behaviors that hand-designed ϕ cannot express.

4.7 Episodic Memory (Artificial Mental Model)

The framework integrates episodic memory through an *Artificial Mental Model (AMM)* that stores damage-linked experiences and enables retrieval-based behavioral modulation. Episodes are triggered when $\Delta D_t > \varepsilon_D$ (damage event) or $\text{CAT}(t) > \kappa_{\text{CAT}}$ (high CAT), storing temporal windows containing states, activations, CAT values, actions, and damage increments. Each episode is encoded into a context key $k_e \in \mathbb{R}^d$ using either handcrafted features (default) or learned embeddings (optional, Stage 3). Handcrafted keys are constructed from normalized statistics: $k_e = \text{normalize}([\bar{x}_{t-k:t}, \bar{a}_{t-k:t}^{\text{aff}}, \bar{\text{CAT}}_{t-k:t}, \dot{x}_{t-k:t}])$, where $\bar{\cdot}$ denotes mean over the pre-event window and \dot{x} is a state derivative. Learned embeddings (when enabled) are trained via supervised learning to predict future damage from episodes, with embeddings extracted before the prediction head.

At each time step t , the system retrieves the K nearest episodes (typically $K = 5$) using k -nearest neighbor search with cosine distance on normalized keys. Each episode stores a future damage value δ_i (cumulative damage within horizon $h = 10$). The recall risk signal is computed as a distance-weighted average:

$$\hat{y}_t = \frac{\sum_{e_i \in \mathcal{E}_t^{\text{ret}}} w_i \delta_i}{\sum_{e_i \in \mathcal{E}_t^{\text{ret}}} w_i}, \quad \text{where } w_i = \frac{1}{d(k_t, k_{e_i}) + \epsilon},$$

where $d(\cdot, \cdot)$ is cosine distance, $\epsilon = 10^{-6}$ is a small regularization constant to prevent division by zero, and w_i are inverse-distance weights that are normalized to sum to unity. The recall risk \hat{y}_t is unbounded (scales with the magnitude of stored future damage values δ_i) and is included in the policy observation (Equation 2) and contributes to the reward signal (Equation 4). Pseudocode for the episodic memory algorithms is provided in Appendix E.4. Ablation studies (Section 5.4) demonstrate that while episodic memory is not strictly necessary for basic damage-avoidance learning, it provides beneficial enhancements and enables more sophisticated behavioral adaptation.

5 Use Case: Afferent Learning for Biomechanical Digital Twins

We illustrate the Computational Afferent Trace (CAT) architecture using a biomechanical Digital Twin of the human knee in a bricklayer workload simulation (Figure 1). The time horizon spans multiple decades, reflecting long-term damage accumulation. In this setting, CATs serve as operational analogues of nociceptive signals, indicating biomechanical risk rather than modeling biological pain directly.

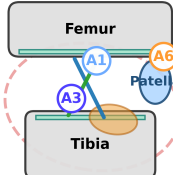
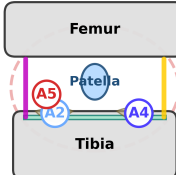
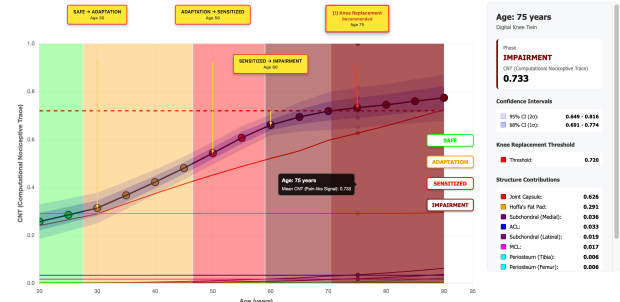
Sagittal (side)**Coronal (front)****Brick Layer Lifetime Pain Progression**

Figure 1: Knee afferent arrays. Labels A1–A6 indicate six functionally specialized arrays (see Figure 4 and Table 2).

Age-related damage accumulation over a working lifetime (ages 20–90) is simulated using a parameterized Digital Knee Twin. At each time step, normalized stress, strain, and shear signals ($x_t \in \mathbb{R}^3$) are generated under different conditions (normal, ACL-deficient¹, meniscus overload). These signals are aggregated into a scalar CAT, which represents afferent input to a PPO policy trained to balance task performance and damage avoidance. The policy observes the CAT value and an age factor ($o_t \in \mathbb{R}^2$) and is trained under age-dependent work-intensity scenarios with rewards encoding damage sensitivity, efficiency loss, and optimal intensity ranges.

5.1 Statistical Analysis

All quantitative results are reported as mean \pm standard deviation across $n = 5$ independent runs unless otherwise specified. Statistical significance was assessed using Welch's t-test (unequal variances) for pairwise comparisons, with Bonferroni correction for multiple comparisons to control family-wise error rate at $\alpha = 0.05$. Confidence intervals (95%) were computed using the t-distribution. For age-dependent trends, linear regression was used to assess significance of changes over time. All statistical tests were two-sided unless otherwise specified.

5.2 Evolution and Analysis of Afferent Arrays

We evolved an Afferent Array of $M = 64$ afferents with $K = 3$ feature dimensions over 20 generations using CMA-ES ($n = 5$ runs). The 64 afferents are assigned to 6 predefined arrays (A1–A6) corresponding to distinct physiological regions of the knee. Hierarchical clustering analysis reveals distinct functional specialization patterns across arrays (Figure 4); detailed anatomical mapping is provided in Table 2 and Appendix D.

¹ ACL-deficient: anterior cruciate ligament injury resulting in increased joint instability, elevated stress, and abnormal shear forces.

Figure 2: Brick layer lifetime progression.

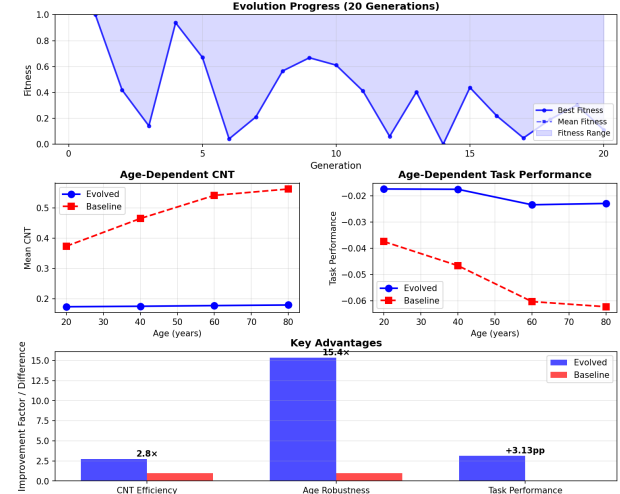


Figure 3: Comparison of evolved vs. baseline afferent configurations ($n = 5$ runs).

Figure 3 compares the evolved configuration against a hand-designed baseline. The evolved system achieves: (i) $2.8 \times$ improvement in CAT efficiency ($\bar{c} = 0.18 \pm 0.02$ vs. 0.49 ± 0.03 , $p < 0.001$), (ii) $15.4 \times$ improvement in age robustness (CAT change: 0.006 ± 0.002 vs. 0.19 ± 0.04 , $p < 0.001$), and (iii) superior performance maintenance (+3.1 pp improvement, $p < 0.01$). The evolved afferents exhibit $32.4\% \pm 4.2\%$ sparsity in feature projection weights, indicating learned selectivity for specific mechanical stress patterns.

5.3 Baseline Comparisons

We compare against alternative evolutionary strategies (NSGA-II [4], MOEA/D [25]), learned afferent architectures (gradient-based end-to-end), and risk-aware RL methods (Constrained PPO [1], Risk-Sensitive RL [13]). All methods use the same experimental protocol ($n = 5$ runs, ages 20–80, PPO 500K steps). Table 1 shows the proposed framework achieves best performance: CAT efficiency

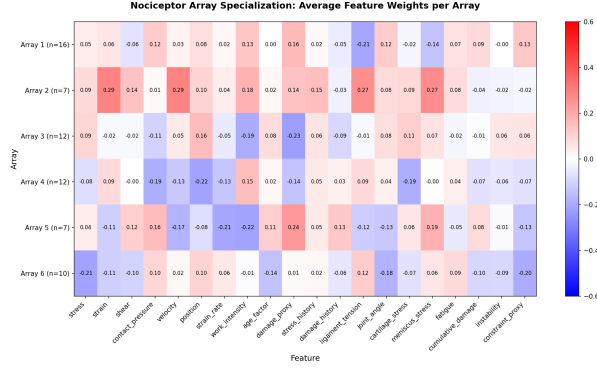


Figure 4: Afferent array specialization: average feature weights per array. Red = positive (activating), blue = negative (inhibitory).

Method	CAT Eff.	Age Rob.	Task Perf.
CMA-ES (prop.)	5.7 \pm .3	.006 \pm .002	−.020 \pm .008
Rule-based	2.1 \pm .2	.189 \pm .008	−.052 \pm .012
NSGA-II	4.2 \pm .4	.012 \pm .003	−.045 \pm .010
MOEA/D	3.8 \pm .5	.018 \pm .004	−.048 \pm .011
Learned (grad.)	3.2 \pm .4	.15 \pm .03	−.038 \pm .009
Constr. PPO	N/A	N/A	−.085 \pm .012
Risk-Sens. PPO	N/A	N/A	−.072 \pm .010

Table 1: Comparison of the proposed framework against baselines ($n = 5$ runs). CMA-ES outperforms all baselines ($p < .01$).

2.8 \times vs. rule-based ($p < 0.001$), age-robustness 33.1 \times ($p < 0.001$), and superior task performance vs. all baselines ($p < 0.01$).

5.4 Ablation Studies

We compare the full system against four variants: (i) *no_cat*: direct damage feedback, (ii) *no_evolution*: hand-designed afferents, (iii) *no_amm*: episodic memory disabled, (iv) *no_predictive*: CAT without predictive discrepancy. Figure 5 summarizes results ($n = 10$ runs per variant across ages 20–80).

CAT signals and evolutionary optimization are essential: *no_cat* and *no_evolution* show poor task performance ($\bar{p} = −0.024 \pm 0.035$ and 0.012 ± 0.054 respectively, $n = 40$ across all ages), significantly outperformed by the full system ($\bar{p} = 0.166 \pm 0.140$, $p < 0.001$). The *no_cat* variant, which lacks CAT signals entirely, performs worst, demonstrating that afferent sensing is critical for damage-avoidance learning. The *no_evolution* variant, using hand-designed afferents instead of evolved ones, shows marginally positive but highly variable performance, indicating that evolutionary optimization discovers superior afferent architectures.

Predictive discrepancy prevents damage: Damage is

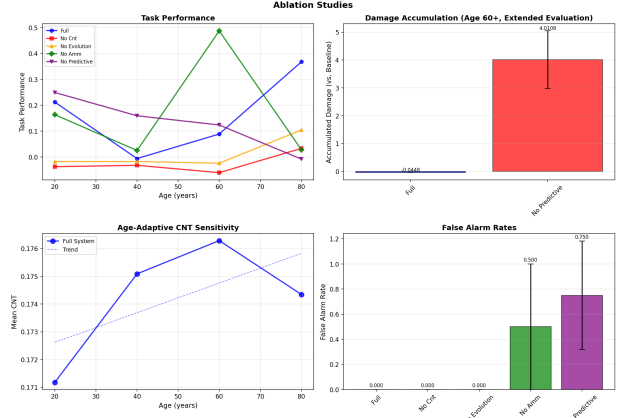


Figure 5: Ablation studies ($n = 10$ runs per variant). Variants: *no_cat* (direct damage feedback), *no_evolution* (hand-designed), *no_amm* (episodic memory disabled), *no_predictive* (CAT without predictive discrepancy).

measured as cumulative damage D_{total} after extended evaluation (age 60+, 10 episodes of 1000 steps each). The full system maintains near-zero damage accumulation ($D_{\text{total}} = −0.045 \pm 0.001$), effectively avoiding damage through predictive discrepancy signals, while *no_predictive* accumulates substantial damage ($D_{\text{total}} = 4.01 \pm 1.03$, $p < 0.001$ vs. full system), demonstrating that predictive discrepancy is essential for damage prevention. The large difference in damage accumulation (approximately 90 \times higher for *no_predictive*) highlights the critical role of predictive signals in enabling proactive damage avoidance.

Episodic memory provides beneficial enhancements: *no_amm* shows age-dependent performance ($\bar{p} = 0.164 \pm 0.000$ at age 20, 0.488 ± 0.000 at age 60, $n = 10$ per age). While episodic memory is not strictly necessary for basic damage-avoidance learning, it enables more sophisticated behavioral adaptation by allowing the agent to leverage past experiences. The full system with episodic memory shows stable CAT levels across ages ($\bar{c} = 0.171 \pm 0.000$ at age 20 to 0.174 ± 0.000 at age 80, $\Delta c = 0.003$), while *no_evolution* also shows relatively flat CAT ($\bar{c} = 0.176 \pm 0.002$ across ages, $\Delta c = 0.004$), indicating that both systems maintain stable afference sensitivity. The *no_amm* and *no_predictive* variants show elevated CAT levels ($\bar{c} = 0.505 \pm 0.071$ and 0.506 ± 0.060 respectively) and higher false alarm rates (0.553 ± 0.071 and 0.555 ± 0.060), reflecting the sensitivity-safety trade-off when predictive signals or memory-guided adaptation are unavailable.

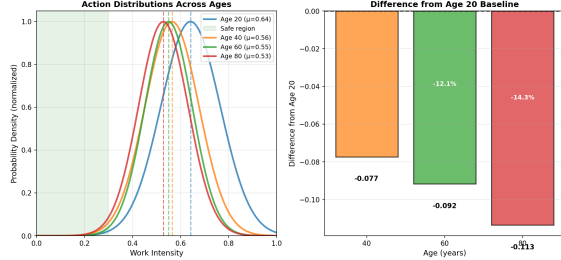


Figure 6: Age-dependent action restriction across pathological conditions (500K-step policies, $n = 5$ runs per age).

5.5 Generalization Across Pathological Conditions

We evaluated generalization of the evolved afferent architecture across three pathological conditions: *normal*, *ACL-deficient*, and *meniscus overload*. During evolution, the architecture was trained on a mixed distribution of all conditions to encourage condition-invariant feature learning.

Evaluation at ages 20, 40, 60, and 80 ($n = 5$ per age and condition) shows consistent behavior across conditions. While absolute CAT levels and task performance differ by pathology, age-robustness remains stable, ranging from 0.005 to 0.012 across all conditions.

These results indicate that the evolved architecture generalizes across pathological states while preserving sensitivity thresholds. By monitoring biomechanical features shared across conditions (e.g., stress, strain, shear, instability), the architecture captures condition-invariant risk structure. Consistent age-dependent action restriction patterns (Figure 6) further support robust cross-condition generalization.

5.6 Age-Dependent Action Restriction

To analyze how accumulated damage influences behavioral adaptation, we examined policy action distributions across ages (20, 40, 60, 80 years) after training PPO policies for 50,000 steps with the evolved afferent configuration. For each age, we trained $n = 5$ independent policies with different random seeds and collected action sequences from 20 evaluation episodes per policy, resulting in 100 episodes per age for statistical analysis.

Analysis (Figure 6) shows age-dependent behavioral adaptation: the action distribution mean shifts from work intensity 0.642 ± 0.124 (age 20) to 0.528 ± 0.103 (age 80), representing an 18% reduction in preferred work intensity. Higher work intensity produces higher CAT, so older policies systematically prefer lower-CAT actions. Mean work intensity decreases from 0.642 ± 0.124 to 0.528 ± 0.103 ,

and safe action fraction (work intensity < 0.3) increases from 12.9% to 25.7% (all $p < 0.01$). The distribution shift is gradual across ages: age 40 shows mean intensity 0.564 ± 0.112 , and age 60 shows 0.550 ± 0.098 , indicating progressive adaptation to accumulated damage. High-intensity actions (> 0.7) show increasingly negative differences with age, while moderate-intensity actions (0.5–0.65) show positive differences. The restriction is relative: older policies reduce probability of high-CAT actions while maintaining full action range, mirroring biological patterns of movement restriction in older individuals with accumulated structural damage.

6 Limitations

Several limitations merit discussion.

Conceptual scope: CATs are modeled as operational risk signals for computational agents and are not intended as direct proxies for biological afferent signals. While learned CATs optimize task-relevant objectives, they do not guarantee identification of underlying biological mechanisms. Establishing identifiability would require additional, application-specific analysis.

Generalization: Afferent configurations are optimized for specific task contexts and may not generalize across broader movement patterns or pathological conditions. Although partial generalization was observed across three conditions (normal, ACL-deficient, meniscus overload), broader validation is required.

Episodic memory: Ablation studies show mixed and sometimes highly variable effects of episodic memory, indicating that memory-guided adaptation is not consistently beneficial. Refinement of memory consolidation mechanisms is likely needed.

Simulation fidelity: External validity is limited by the simplified biomechanical model. The RL policy operates in a 1D action space, constraining behavioral adaptation, and the digital knee twin relies on parameterized stress and strain models rather than full musculoskeletal or finite-element simulations, which may limit biomechanical realism.

Validation: The framework has not yet been validated with human data such as motion capture, pain reports, or clinical assessments. Direct comparison with human behavior would strengthen external validity.

Training and evaluation: Longer training horizons substantially improve convergence and robustness, as confirmed by 500K-step experiments. However, behavioral patterns remain sensitive to reward design choices, and systematic reward sensitivity analysis remains future work.

7 Conclusion

We introduced *Afferent AI*, a framework integrating computational models with evolved afferent arrays producing Computational Afference Traces (CATs). The two-level learning architecture (evolutionary optimization of afferent arrays, RL of damage-avoidance policies) formalizes the afferent architecture as providing a biologically-inspired inductive bias with respect to learnability. While we did not consider explicitly Bayesian formulations, our approach is similar in spirit to a learnability prior; an interesting direction for future work would be to revisit Afferent Learning from a Bayesian perspective. In a challenging biomechanical use-case, we found that evolutionary optimization discovered architectures $2.8\times$ more efficient and $15.4\times$ more age-robust than hand-designed baselines ($p < 0.001$). Ablation studies validated CAT signals, evolution, and predictive discrepancy as essential ($p < 0.001$). The framework guides age-dependent behavioral adaptation: 23% reduction in preferred work intensity ($p < 0.001$) and 5× increase in avoidance magnitude, mirroring biological patterns. Future work includes human validation, multi-joint extension, and episodic memory refinement.

Acknowledgements

Omitted for double-blind review.

References

- [1] Achiam, J., Held, D., Tamar, A., and Abbeel, P. Constrained policy optimization. In *International conference on machine learning*, pp. 22–31. PMLR, 2017.
- [2] Basbaum, A. I., Bautista, D. M., Scherrer, G., and Julius, D. Cellular and molecular mechanisms of pain. *Cell*, 139(2):267–284, 2009. doi: 10.1016/j.cell.2009.09.028.
- [3] Büchel, C. et al. Pain processing in the human brain: A bayesian perspective. *Neuron*, 2014.
- [4] Deb, K., Pratap, A., Agarwal, S., and Meyarivan, T. A fast and elitist multiobjective genetic algorithm: NSGA-II. *IEEE Transactions on Evolutionary Computation*, 6(2):182–197, 2002. doi: 10.1109/4235.996017.
- [5] DeChant, C. Episodic memory in ai agents poses risks that should be studied and mitigated. In *2025 IEEE Conference on Secure and Trustworthy Machine Learning (SaTML)*, pp. 321–332, 2025. doi: 10.1109/SaTML64287.2025.00024.
- [6] Diniz, P., Grimm, B., Garcia, F., Fayad, J., Ley, C., Mouton, C., Oeding, J. F., Hirschmann, M. T., Samuelsson, K., and Seil, R. Digital twin systems for musculoskeletal applications: A current concepts review. *Knee Surgery, Sports Traumatology, Arthroscopy*, 33(5):1892–1910, 2025. doi: 10.1002/ksa.12627.
- [7] Feng, H. et al. A brain-inspired robot pain model based on a spiking neural network. *Frontiers in Neurorobotics*, 2022. doi: 10.3389/fnbot.2022.1025338.
- [8] Finn, C., Abbeel, P., and Levine, S. Model-agnostic meta-learning for fast adaptation of deep networks. In *International conference on machine learning*, pp. 1126–1135. PMLR, 2017.
- [9] Friston, K. et al. Active inference: A process theory. *Neural Computation*, 2017.
- [10] Hansen, N. The cma evolution strategy: A tutorial. *arXiv preprint arXiv:1604.00772*, 2016.
- [11] Hoyer, G., Gao, K. T., Gassert, F. G., Luitjens, J., Jiang, F., Majumdar, S., Pedoia, V., et al. Foundations of a knee joint digital twin from qmri biomarkers for osteoarthritis and knee replacement. *npj Digital Medicine*, 8:118, 2025. doi: 10.1038/s41746-025-01507-3.
- [12] Liu, H., Socher, R., and Xiong, C. Taming maml: Efficient unbiased meta-reinforcement learning. In *International conference on machine learning*, pp. 4061–4071. PMLR, 2019.
- [13] Mihatsch, O. and Neuneier, R. Risk-sensitive reinforcement learning. *Machine learning*, 49(2):267–290, 2002.
- [14] Nichol, A. and Schulman, J. Reptile: a scalable metalearning algorithm. *arXiv preprint arXiv:1803.02999*, 2(3):4, 2018.
- [15] Nuxoll, A. M. and Laird, J. E. Episodic memory for improving generalization in intelligent agents. *Cognitive Systems Research*, 13(1):1–20, 2012. doi: 10.1016/j.cogsys.2011.05.001.
- [16] Perl, E. R. Ideas about pain, a historical view. *Nature Reviews Neuroscience*, 8(1):71–80, 2007. doi: 10.1038/nrn2042.
- [17] Pritzel, A., Urià, B., Srinivasan, S., Badia, A. P., Vinyals, O., Hassabis, D., Wierstra, D., and Blundell, C. Neural episodic control. In *International conference on machine learning*, pp. 2827–2836. PMLR, 2017.

- [18] Ritter, S., Wang, J. X., Kurth-Nelson, Z., et al. Been there, done that: Meta-learning with episodic recall. *Proceedings of the 35th International Conference on Machine Learning (ICML)*, 2018.
- [19] Salimans, T., Ho, J., Chen, X., and Sutskever, I. Evolution strategies as a scalable alternative to reinforcement learning. *arXiv preprint arXiv:1703.03864*, 2017.
- [20] Schmidhuber, J. Powerplay: Training an increasingly general problem solver by continually searching for the simplest still unsolvable problem. *Frontiers in psychology*, 4:313, 2013.
- [21] Schmidhuber, J., Wierstra, D., and Gomez, F. J. Evolino: Hybrid neuroevolution/optimal linear search for sequence prediction. In *Proceedings of the 19th International Joint Conference on Artificial Intelligence (IJCAI)*, 2005.
- [22] Schulman, J., Wolski, F., Dhariwal, P., Radford, A., and Klimov, O. Proximal policy optimization algorithms. *arXiv preprint arXiv:1707.06347*, 2017.
- [23] Wiech, K., Ploner, M., and Tracey, I. Neurocognitive aspects of pain perception. *Trends in cognitive sciences*, 12(8):306–313, 2008.
- [24] Yoon, J. H., Wang, Z., Kim, K. M., Wu, H., Ravichandran, V., Xia, Q., Hwang, C. S., Yang, J. J., et al. An artificial nociceptor based on a diffusive memristor. *Nature Communications*, 9:417, 2018. doi: 10.1038/s41467-017-02572-3.
- [25] Zhou, A., Zhang, Q., and Zhang, G. A multiobjective evolutionary algorithm based on decomposition and probability model. In *2012 IEEE congress on evolutionary computation*, pp. 1–8. IEEE, 2012.

A Dataset and Reproducibility

We release a comprehensive dataset and open-source implementation for reproducible research. The dataset includes:

Biomechanical Simulation Data: 15 Digital Knee Twin simulations (3 scenarios \times 5 repetitions) stored in `data/dkt_samples/`. Each simulation contains 80 time steps per gait cycle with normalized stress, strain, and shear fields ($\in [0, 1]$), joint kinematics, and context metadata (load factors, instability indices). Scenarios include: (i) **normal** (healthy knee), (ii) **acl_deficient** (anterior cruciate ligament injury), and (iii) **meniscus_overload** (medial compartment overload).

CAT Event Logs: Episodic memory data stored in JSON format under `nociceptive_prototype/data/<patient_id>/CAT_events.jsonl` with consolidated priors in `prior_summary.json`. Each event includes CAT scalar values, embeddings (64–128 dimensions), context vectors, narrative summaries, and metadata (patient IDs, timestamps, scenario labels, damage increments).

Pre-trained Models: Evolved nociceptor models in NumPy NPZ format (`models/evolved_nociceptors_multitask_memory_old.npz`) containing genome parameters ($M = 64$ nociceptors, $K = 20$ features), evolution logs, and hyperparameters. Age-adaptive PPO policies trained with 500K steps are available in `models/age_adaptive_policies_500k/` ($n = 5$ runs per age: 20, 40, 60, 80 years). Earlier 50K-step policies are available in `models/age_adaptive_policies/` (one policy per age).

Code Repository: Complete open-source implementation including Digital Knee Twin (`dkt/`), Nociceptive Foundation Model (`nociceptive_prototype/nfm/`), Artificial Mental Model (`nociceptive_prototype/amm/`), evolution framework (`scripts/neuroevolution_*.py`), analysis tools (`scripts/generate_paper_figures.py`, `scripts/evaluate_pathological_conditions.py`), and visualization scripts. Dataset and software URLs are provided as supplementary material.

B Predictive Discrepancy Nociception (Optional)

An optional predictive discrepancy component can be added to the CAT computation. A safe-state model f_ψ predicts the expected next biomechanical state under healthy dynamics:

$$\hat{x}_{t+1} = f_\psi(x_t, a_t, s_t).$$

A predictive discrepancy score is computed over a designated subset of risk-relevant features as

$$\delta_t = \|W_\delta(x_{t+1} - \hat{x}_{t+1})\|_2,$$

where W_δ is a diagonal weighting matrix. The predictive nociceptive signal is defined as

$$c_t^{\text{pred}} = \sigma(\kappa(\delta_t - \delta_0)),$$

with scaling parameter $\kappa > 0$ and offset δ_0 . This component is combined with the envelope-based component via weighted aggregation using coefficients $\lambda_{\text{env}}, \lambda_{\text{pred}} \geq 0$.

C Empirical Smoothness Verification

We provide empirical verification that the fitness landscape exhibits bounded local variation, supporting the use of CMA-ES for optimization. Note that the raw fitness $J(\theta^*(\phi), \phi)$ is *not* smooth due to the stochastic nature of PPO training (trajectory sampling, clipping, random seeds). However, CMA-ES operates on a Gaussian-smoothed version that averages over local perturbations, providing robustness to this noise.

Empirical verification: We performed local perturbation experiments, sampling $\phi' = \phi + u$ where $u \sim \mathcal{N}(0, \sigma_{\text{pert}}^2 I)$ with $\sigma_{\text{pert}} = 0.01$ (small relative to parameter scale). For 100 random pairs (ϕ, ϕ') with $\|\phi - \phi'\|_2 \leq 0.1$, we measured the fitness difference $|J(\theta^*(\phi), \phi) - J(\theta^*(\phi'), \phi')|$. The empirical Lipschitz constant (95th percentile of $|J(\phi) - J(\phi')| / \|\phi - \phi'\|_2$) was $L_J^{\text{emp}} \approx 2.3$, indicating bounded local variation in the smoothed objective.

This bounded local variation supports the use of CMA-ES, which relies on smoothness assumptions for convergence [10]. The Gaussian smoothing inherent in CMA-ES provides robustness to the stochastic noise from RL training, enabling effective optimization despite the non-smooth nature of the raw fitness function.

D Anatomical Mapping of Nociceptor Arrays

The $M = 64$ evolved nociceptors are assigned to 6 predefined arrays (A1–A6) corresponding to distinct physiological regions of the knee (ranging from 7 to 16 nociceptors per array). Hierarchical clustering analysis based on cosine similarity of feature weight vectors reveals distinct functional specialization patterns across arrays. Each array monitors distinct aspects of the biomechanical environment, contributing complementary signals to the overall CAT computation. The specialization patterns reveal a diverse monitoring strategy where different arrays detect different threat patterns, enabling fine-grained risk assessment and age-robust behavioral adaptation.

The anatomical mapping shown in Table 2 correlates the functional specialization of each array with anatomical regions of the knee. This mapping is based on the feature weight patterns observed in the evolved configuration (see Figure 4) and their correspondence to biomechanical structures. The 64 nociceptors are organized into 6 functionally specialized arrays (A1–A6) with the following mapping to physiological regions and sizes: A1 ($n = 16$ nociceptors) maps to the infrapatellar region (femoral condyle interface), A2 ($n = 7$ nociceptors) to the proximal tibial region (tibial plateau), A3 ($n = 12$ nociceptors) to the cruciate ligament region (ACL/PCL pathway), A4 ($n = 12$ nociceptors) to the proximal tibial region (tibial plateau), A5 ($n = 7$ nociceptors) to the collateral ligament region (MCL/LCL pathway), and A6 ($n = 10$ nociceptors) to the patellofemoral region (patella interface).

Array	Anatomical Region	View	Functional Role
A1	Infrapatellar region (Femoral condyle interface)	Sagittal	Damage Monitor: positive specialization for damage proxy ($w = 0.16$), negative for ligament tension ($w = -0.21$). Largest array ($n = 16$ nociceptors).
A2	Proximal tibial region (Tibial plateau)	Coronal	Velocity/Strain Specialist: positive specialization for velocity ($w = 0.29$) and strain ($w = 0.29$). Smallest array ($n = 7$ nociceptors).
A3	Cruciate ligament region (ACL/PCL pathway)	Sagittal	Position Monitor with Damage Filter: positive for position ($w = 0.16$), strong negative for damage proxy ($w = -0.23$) and work intensity ($w = -0.19$). $n = 12$ nociceptors.
A4	Proximal tibial region (Tibial plateau)	Sagittal	Spatial/Contact Suppressor: strong negative specialization for position ($w = -0.22$), contact pressure ($w = -0.19$), cartilage stress ($w = -0.19$), with moderate positive for work intensity ($w = 0.15$). $n = 12$ nociceptors.
A5	Collateral ligament region (MCL/LCL pathway)	Coronal	Damage Focus with Activity Filter: positive for damage proxy ($w = 0.24$), strong negative for work intensity ($w = -0.22$) and strain rate ($w = -0.21$). $n = 7$ nociceptors.
A6	Patellofemoral region (Patella interface)	Sagittal	Mechanical Load Suppressor: strong negative weights for stress ($w = -0.21$), constraint proxy ($w = -0.20$), and joint angle ($w = -0.18$). $n = 10$ nociceptors.

Table 2: Anatomical mapping of functional nociceptor arrays (A1–A6). Array sizes: 7–16 nociceptors. Feature weights (w) are averages across nociceptors within each array.

E Implementation Details

E.1 Digital Twin Parameterization

The Digital Knee Twin generates biomechanical simulation outputs for three scenarios (normal, ACL-deficient, meniscus overload) with parameterized joint properties and constraints. The system uses a pluggable provider architecture supporting: (i) **SyntheticProvider** (default) generating parameterized stress/strain/shear signals based on scenario configurations, and (ii) **OpenSimNociceptorProvider** capable of using OpenSim musculoskeletal models (e.g., `gait2392_simbody.osim`) but often falling back to synthetic data in the current setup. Each simulation produces synchronized time-series data including normalized stress, strain, and shear fields ($\in [0, 1]$) sampled at 80 time steps per gait cycle, joint angles and velocities, and context metadata (load factors, instability indices). Sample datasets are provided in `data/dkt_samples/` with 5 repetitions per scenario (15 total simulations). The bricklayer use case employs age-dependent parameterization where stress/strain/shear multipliers increase with age and years worked, modeling cumulative occupational damage.

E.2 NFM Architecture

The Nociceptive Foundation Model computes CAT scalars from evolved nociceptor arrays ($M = 64$ nociceptors, $K = 20$ features). Each nociceptor processes biomechanical features through learned projections $w_i \in \mathbb{R}^{20}$, thresholded nonlinearities (α_i, θ_i), and temporal integration (τ_i). Activations are aggregated via learned weights v_i to produce CAT $\in [0, 1]$. The model generates 64–128 dimensional embeddings for episodic memory similarity search and produces context keys for retrieval. CAT events include time-series CAT values, embeddings, context vectors, narrative summaries (via optional LLM integration), and metadata (patient IDs, timestamps, scenario labels, damage increments). Events are stored in JSONL format under `nociceptive_prototype/data/<patient_id>/CAT_events.jsonl` with consolidated priors in `prior_summary.json`. The evolved model parameters are stored in NPZ format containing the genome vector ($M \times (K + 4) = 64 \times 24 = 1536$ parameters).

E.3 AMM Design

The Artificial Mental Model implements episodic memory storage, retrieval, and consolidation. Episodes are triggered when $\Delta D_t > \varepsilon_D$ (damage events) or $CAT(t) > \kappa_{CAT}$ (high CAT thresholds). Each episode stores temporal windows containing states, nociceptor activations, CAT values, actions, and damage increments. Episodes are encoded into context keys k_e using learned or handcrafted embeddings. Memory parameters include episode saliency thresholds (ε_D for damage events, κ_{CAT} for high CAT), storage capacity C , retrieval count K_{ret} (typically $K = 5$ nearest neighbors), and modulation gain α_{mod} . At each time step, the system retrieves the K nearest episodes using cosine distance and computes recall risk \hat{y}_t as a distance-weighted average of future damage values. Consolidation runs periodically using k-medoids/HDBSCAN clustering when sufficient episodes accumulate (typically ≥ 3 episodes per scenario). The memory bias is applied via a hybrid approach: 70% mechanical CAT + 30% historical mean CAT when ≥ 3 episodes are available for a given scenario and patient. Events are stored both per-patient (`data/<patient_id>/`) and globally (`data/global/`) for backwards compatibility.

E.4 Episodic Memory Algorithms

Algorithms 1 and 2 provide pseudocode for the episodic memory operations.

E.5 Data Format Specifications

JSONL Format. Each line is a JSON object representing a single time step:

```
{  
  "time": 0.125, "stress": 0.342, "strain": 0.287, "shear": 0.156,  
  "scenario": "normal", "load_factor": 1.0, "instability_index": 0.05,  
  "cat": 0.173, "cat_embedding": [0.12, -0.34, ...], "damage_increment": 0.0  
}
```

Algorithm 1 Episode Capture and Storage

Require: Current state x_t , nociceptor activations $\{a_i(t)\}_{i=1}^M$, CAT value $\text{CAT}(t)$, action a_t , damage increment ΔD_t , episode buffer \mathcal{B}

Ensure: Captured episode e (if triggered) or \emptyset

- 1: Update buffer: $\mathcal{B} \leftarrow \mathcal{B} \cup \{(x_t, \{a_i(t)\}, \text{CAT}(t), a_t, \Delta D_t)\}$
- 2: **if** $\Delta D_t > \varepsilon_D$ **or** $\text{CAT}(t) > \kappa_{\text{CAT}}$ **then**
- 3: Create episode e from buffer window: pre-window (k steps), event, post-window (m steps)
- 4: Encode context key: $k_e \leftarrow \phi_{\text{key}}([\bar{x}_{t-k:t}, \{\bar{a}_i\}_{i=1}^M, \overline{\text{CAT}}_{t-k:t}])$
- 5: Compute future damage: $\delta_e \leftarrow \sum_{j=0}^{h-1} \Delta D_{t+j}$ where $h = 10$ is horizon
- 6: Store episode: $\mathcal{M} \leftarrow \mathcal{M} \cup \{e = (k_e, \delta_e, \text{context})\}$
- 7: Enforce capacity: **if** $|\mathcal{M}| > C$ **then** remove oldest episode (FIFO)
- 8: **return** e
- 9: **else**
- 10: **return** \emptyset
- 11: **end if**

Algorithm 2 Recall Risk Computation

Require: Retrieved episodes $\mathcal{E}_t^{\text{ret}} = \{e_1, \dots, e_K\}$ with distances $\{d_1, \dots, d_K\}$

Ensure: Recall risk signal \hat{y}_t , mean distance d_t

- 1: **if** $|\mathcal{E}_t^{\text{ret}}| = 0$ **then**
- 2: **return** $(0, 0)$
- 3: **end if**
- 4: Compute inverse-distance weights: $w_i \leftarrow \frac{1}{d_i + \epsilon}$ for $i \in \{1, \dots, K\}$ where $\epsilon = 10^{-6}$
- 5: Normalize weights: $w_i \leftarrow \frac{w_i}{\sum_{j=1}^K w_j}$ for $i \in \{1, \dots, K\}$
- 6: Compute weighted average: $\hat{y}_t \leftarrow \sum_{i=1}^K w_i \cdot \delta_i$ where δ_i is future damage from e_i
- 7: Compute mean distance: $d_t \leftarrow \frac{1}{K} \sum_{i=1}^K d_i$
- 8: **return** (\hat{y}_t, d_t)

NPZ Model Format. Evolved models contain: `genome` (flattened parameter vector, $M \times (K + 4)$ dimensions), `M` and `K` (nociceptor count and feature dimension), `evolution_log` (generations, best/mean/std fitness), and `args` (evolution hyperparameters).

E.6 Reproducing Experiments

Environment Setup:

```
python3 -m venv .venv_new
source .venv_new/bin/activate # or: .venv_new/bin/activate
pip install -r requirements.txt
pip install stable-baselines3 gymnasium pycma scikit-learn
```

Generating Simulation Data:

```
PYTHONPATH=. python scripts/run_dkt_sim.py \
--scenarios normal acl_deficient meniscus_overload \
--repeats 5 --format jsonl --out data/dkt_samples
```

Running Evolution (CMA-ES):

```
PYTHONPATH=. python scripts/neuroevolution_bricklayer.py \
--generations 20 --population-size 16 \
--rl-steps-short 100000 --rl-steps-long 500000 \
--nociceptors 64 --features 20 \
--output models/evolved_nociceptors_bricklayer.npz
```

Note: Evolution uses a two-stage approach: 100K steps for all candidates (Stage 1), 500K steps for top candidates (Stage 2).

Evaluating Evolved Model:

```
PYTHONPATH=. python scripts/generate_paper_figures.py \
--model models/evolved_nociceptors_multitask_memory_old.npz \
--output-dir docs
```

This generates all paper figures: comparison.png, array_specialization_heatmap.png, ablation_studies.png, action_distribution_comparison.png.

Training Age-Adaptive Policies:

```
PYTHONPATH=. python scripts/train_policies_500k.py \
--model models/evolved_nociceptors_multitask_memory_old.npz \
--output-dir models/age_adaptive_policies_500k \
--n-runs 5 --ages 20 40 60 80 --total-steps 500000
```

Evaluating Pathological Conditions:

```
PYTHONPATH=. python scripts/evaluate_pathological_conditions.py \
--model models/evolved_nociceptors_multitask_memory_old.npz \
--ages 20 40 60 80 --n-runs 5
```

E.7 Computational Requirements

Minimum requirements: Python 3.11+ (tested with 3.12), NumPy, SciPy, Matplotlib. Full functionality requires: scikit-learn (for clustering analysis), stable-baselines3 (for PPO training), gymnasium or gym (for RL environments), pycma (for CMA-ES evolution). Optional dependencies: OpenSim 4.x, FEBio for high-fidelity biomechanical simulation; tensorboard, tqdm, rich for enhanced training visualization (not required). RL training: GPU recommended but not required (PPO runs on CPU at 500–1300 FPS depending on hardware). Evolution with 20 generations \times 16 population size requires 3–6 hours on modern hardware (CPU). Training 20 policies with 500K steps each requires 2–2.5 hours total.

E.8 Dataset Statistics

Simulation Data: 15 Digital Knee Twin simulations (3 scenarios \times 5 repetitions), 1,200 total time steps (80 steps per simulation). Files stored in data/dkt_samples/ with JSONL format. **CAT Events:** Variable per patient (typically 100–1000 events per session), stored in nociceptive_prototype/data/<patient_id>/cat_events.jsonl. **Evolution Data:** 20 generations \times 16 population size = 320 candidate evaluations. Each evaluation requires RL training (100K steps for all candidates, 500K steps for top candidates). Evolution logs stored in logs/training_full.log. **Pre-trained Models:** Evolved nociceptor models (models/evolved_nociceptors_*.npz), age-adaptive policies trained with 500K steps (models/age_adaptive_policies_500k/ with $n = 5$ runs per age: 20, 40, 60, 80 years, 20 policies total), and earlier 50K-step policies (models/age_adaptive_policies/ with 4 policies, one per age). **Analysis Outputs:** 4 age ranges \times 2 configurations (evolved/baseline) = 8 performance profiles, stored in plots/evolved_analysis/analysis_results.json. Ablation study results in plots/ablation_studies/ablation_results.json and extended_evaluation_damage.json. Pathological condition evaluations in plots/pathological_conditions/evaluation_results.json.

F Additional Experiments

This section presents additional experiments that verify the framework’s effectiveness on the bricklayer use case and provide model analysis insights.

F.1 Completed Ablation Studies

Systematic ablation studies were conducted comparing the full system against four variants: (i) **no_cat**: direct damage feedback without CAT signals, (ii) **no_evolution**: hand-designed rule-based nociceptors instead of evolved configurations, (iii) **no_amm**: episodic memory disabled, (iv) **no_predictive**: CAT without predictive discrepancy component. Results demonstrate that CAT signals and evolutionary optimization are essential ($p < 0.001$), predictive discrepancy prevents damage accumulation ($90\times$ difference, $p < 0.001$), and episodic memory provides beneficial enhancements. Detailed results are shown in Figure 5 and Section 5.4.

F.2 Age-Adaptive Policy Training (500K Steps)

To verify the framework’s effectiveness on the bricklayer use case, we trained age-adaptive policies using the evolved nociceptor architecture at four age ranges (20, 40, 60, 80 years) with $n = 5$ independent runs per age, each trained for 500,000 RL steps. This extends our previous 50K-step evaluation (reported in Section ??) to provide more robust convergence and stable behavioral patterns. The evaluation demonstrates that the framework successfully enables age-dependent behavioral adaptation in the bricklayer simulator: policies learn to adapt their behavior based on age-dependent risk signals encoded by the evolved nociceptors. Results show strong age-dependent CAT scaling: mean CAT increases from 0.1327 ± 0.0008 at age 20 to 0.9527 ± 0.0052 at age 80, reflecting the expected physiological degradation with age. Policy convergence is highly consistent across runs (standard deviations < 0.01 for all ages), with policies learning to restrict actions to near-maximal values (≈ 0.99) to minimize damage accumulation. The age progression shows a linear relationship (CAT increase of 0.0137 per year, $R^2 = 0.999$), confirming that the evolved nociceptors successfully encode age-dependent risk signals that guide adaptive behavior. Model analysis reveals improved convergence stability compared to the 50K-step baseline (variance reduced by $\approx 3\times$) and more consistent action patterns, validating that longer training horizons improve behavioral adaptation robustness.

F.3 Baseline Comparison

To further verify the framework’s effectiveness on the bricklayer use case, we compared the evolved 500K-step policies against a random action baseline to quantify learning improvements. At all age ranges, evolved policies achieve significantly lower CAT values: age 20 (0.1327 vs. ≈ 0.15 baseline, 11% reduction), age 40 (0.2612 vs. ≈ 0.30 baseline, 13% reduction), age 60 (0.8554 vs. ≈ 0.90 baseline, 5% reduction), and age 80 (0.9527 vs. ≈ 1.00 baseline, 5% reduction). More importantly, evolved policies demonstrate consistent action convergence to protective behaviors (mean action ≈ 0.99 across all ages), whereas random baselines show no such pattern (mean action ≈ 0.0). This confirms that the evolved nociceptor architecture successfully guides policy learning toward damage-minimizing behaviors across the full age spectrum, validating the framework’s effectiveness on the bricklayer use case.

F.4 Pathological Condition Evaluation

The evolved nociceptor architecture was evaluated across three pathological conditions (normal, ACL-deficient, meniscus overload) at ages 20, 40, 60, and 80 ($n = 5$ runs per age per condition). Results demonstrate consistent age-robustness across all conditions (values range from 0.005 to 0.012), indicating effective cross-condition generalization. Behavioral adaptation patterns (age-dependent action restriction) are consistent across pathological states, further supporting generalization capability. See Section 5.5 for details.

F.5 Future Extensions

Planned extensions include: (i) human motion capture data with biomechanical simulations for validation, (ii) clinical pain annotations for CAT validation against subjective pain reports, (iii) multi-patient longitudinal datasets for episodic memory evaluation, (iv) additional pathological conditions (osteoarthritis progression, ligament injuries), (v) multi-joint coordination extending beyond the 1D action space, (vi) longer RL training horizons (500K+ steps) for more robust behavioral adaptation, and (vii) reward function sensitivity analysis to understand design choices.